Reaction kinetics of ultrathin NaCl films on Ag(001) upon electron irradiation

Ala Husseen, Séverine Le Moal, Hamid Oughaddou, Gérald Dujardin, Andrew Mayne, Eric Le Moal

Reaction kinetics of ultrathin NaCl films on Ag(001) upon electron irradiation

Ala Husseen, Séverine Le Moal, Hamid Oughaddou, Gérald Dujardin, Andrew Mayne, and Eric Le Moal*
Institut des Sciences Moléculaires d'Orsay, CNRS, Univ. Paris-Sud, Université Paris-Saclay, 91405 Orsay, France
(Received 10 February 2017; revised manuscript received 30 November 2017; published 13 December 2017)

We report on an electron-induced modification of alkali halides in the *ultrathin* film regime. The reaction kinetics and products of the modifications are investigated in the case of NaCl films grown on Ag(001). Their structural and chemical modification upon irradiation with electrons of energy 52–60 eV and 3 keV is studied using low-energy electron diffraction (LEED) and Auger electron spectroscopy (AES), respectively. The irradiation effects on the film geometry and thickness (ranging from between two and five atomic layers) are examined using scanning tunneling microscopy (STM). We observe that Cl depletion follows different reaction kinetics, as compared to previous studies on NaCl *thick* films and *bulk* crystals. Na atoms produced from NaCl dissociation diffuse to bare areas of the Ag(001) surface, where they form Na-Ag superstructures that are known for the Na/Ag(001) system. The modification of the film is shown to proceed through two processes, which are interpreted as a *fast* disordering of the film with removal of NaCl from the island edges and a *slow* decrease of the structural order in the NaCl with formation of holes due to Cl depletion. The kinetics of the Na-Ag superstructure growth is explained by the limited diffusion on the irradiated surface, due to aggregation of disordered NaCl molecules at the substrate step edges.

DOI: 10.1103/PhysRevB.96.235418

I. INTRODUCTION

Insulating thin films on metals are key in numerous applications, e.g., microelectronics, catalysis, energy generation, plasmonic sensors. In many fundamental research fields, notably in surface science [1], they serve as model templates and atomically controlled spacers, for the manipulation and study of nanoparticles [2–4], molecules [5–10], or single atoms [11]. Most of the time, chemical stability of insulating thin films upon charged particle irradiation is required, e.g., for characterization using electron spectroscopy and microscopy. In some specific cases, their reactivity may even be turned into a unique opportunity to control matter on a subnanometer scale [12,13]. In this context, understanding the reaction kinetics is central for the control of the reaction products.

Sodium chloride (NaCl) dissociation upon electron irradiation has been observed within different energy ranges, in low-energy electron diffraction (LEED) and Auger electron spectroscopy (AES), as well as reflected electron energy loss microscopy (REELM) and reflection high-energy electron diffraction (RHEED) experiments [14–16]. When exposed to the low-energy electron beam of a LEED, thin NaCl films on an Ag(110) crystal have been shown to transform within a few minutes into 2D periodic arrays of sodium atoms adsorbed on silver [17]. These periodic arrays exhibit the same atomic arrangements as observed when sodium is evaporated directly onto Ag(110) [18,19]. To our knowledge, no studies other than Ref. [17] deal with the electron-induced modification of alkali-halide thin films on fcc metals. It has also been reported that a number of surface reconstructions and 2D alloys can be produced through alkali-metal (Li, Na, K, Rb) deposition on fcc metals (Al, Ni, Cu, Ag, Au), by finely controlling the surface coverage [20–34]. However, it is not known whether these superstructures may be obtained through dissociation of alkali-halide thin films.

The electron-induced dissociation of NaCl has been attributed to the substitution of chloride ions with incident electrons, a process that is also at the origin of color centers (i.e., light absorbing defects) in NaCl crystals [14]. This effect, which is known to occur over a broad energy range, could be used to engineer active areas within insulating layers. However, the kinetics of the electron-induced dissociation of alkali halides in the form of *ultrathin* films, i.e., a few atomic layers in thickness, have rarely been addressed [35,36]; most often, *bulk* crystals and *thick* films (tens to hundreds of nanometers) were considered [14,37]. In the ultrathin film case, the limited amount of reactants and the interactions with the substrate may play a crucial part, thus leading to different reaction kinetics, compared to the bulk crystal and thick film cases. The products of alkali-halide dissociation may be different too, since they may adsorb or even react with the substrate, which can be of a different material, e.g., of a metal, whereas on bulk crystals and thick films the dissociation products inevitably adsorb on the same alkali-halide material.

In this paper, we report on the reaction kinetics of ultrathin NaCl films grown on Ag(001) upon irradiation with the electron beams of a LEED (primary electron energy 52–60 eV) and an AES (3 keV). Here, LEED and AES are used both to induce NaCl dissociation and to monitor the structural and chemical modifications of the sample surface. In addition, scanning tunneling microscopy (STM) is used to compare the topography of the as-grown and irradiated NaCl films. Thus we analyze the reaction kinetics and retrieve the rate constant of Cl depletion, and we propose models for the morphological evolution of the irradiated film and the formation of Na-Ag superstructures.

II. METHODS

All experiments are performed in ultrahigh vacuum. NaCl deposition and LEED/AES operations are conducted at a base pressure of 3×10^{-10} mbar. Thin NaCl films are grown on a single crystal of Ag(001). High substrate temperatures of

*eric.le-moal@u-psud.fr

413 and 500 K increase the NaCl molecule diffusion on silver during the deposition to obtain larger NaCl domains [38,39]. Two different substrate temperatures, used for the NaCl growth, yield different film geometries, as shown below. NaCl is evaporated from an effusion cell heated at a temperature in the range of 756–797 K. The cell temperature and deposition time (in the 10–40 min range) are varied in order to study the effect of the film thickness. In addition, the NaCl film thickness gradually decreases when moving away from the center of the silver crystal, which provides a supplementary way to explore the thickness effect when conducting the LEED and AES measurements.

The geometry of the NaCl films before and after electron irradiation is investigated using a low-temperature STM at 78 K (liquid nitrogen cryostat) and at a base pressure of 1×10^{-10} mbar. Bias voltages U_b refer to the sample voltage with respect to the tip. All STM images are acquired at constant current. When NaCl films are grown at 500 K, the micrometer size of the NaCl islands makes it difficult to accurately determine the island size distribution, due to limited STM scan range. Furthermore, the absolute calibration of the NaCl deposition using a quartz microbalance is hampered by the temperature dependence of molecular sticking factors on surfaces. Thus only the local thickness and geometry of the NaCl islands are assessed from the STM images. In addition, we make semiquantitative comparisons of the nominal thicknesses of the NaCl films, based on the intensity ratio of the chlorine and silver AES peaks. To do so, we use the peak-to-peak intensity of the Cl LVV and Ag M_4NN Auger lines, which lie at 181 and 358 eV, respectively. The Cl/Ag AES peak ratio is taken at time $t = 0$, i.e., before electron irradiation starts to modify the chemical composition. For instance, Cl/Ag($t = 0$) is measured at 0.066 and 0.30 in the center of the two samples imaged by STM in Figs. 1(c) and 1(d), respectively. More detailed technical aspects of the experimental setup, as well as the sample preparation and data analysis methods, can be found in Ref. [40].

III. RESULTS

A. NaCl film geometry before dissociation

In the ultrathin film case, the initial geometry of the irradiated NaCl film is expected to play a part in the reaction kinetics, due to the substrate interaction with the reactants and products of the dissociation reaction. In particular, the film thickness and its continuity, as well as the defects in the as-grown NaCl films, are relevant. We show STM topography images of ultrathin NaCl films used in this study, which differ in nominal thickness and growth temperature. Here, STM measurements are carried out before electron irradiation.

Figures 1(a) and 1(b) show STM topography images of an ultrathin NaCl film grown on Ag(001) at 413 K. The NaCl film consists of islands, which have side lengths in the 100–200 nm range and mainly square or rectangular shapes, with rounded corners for the thinnest of them. The island edges exhibit various orientations with respect to the substrate axes, in agreement with previously reported azimuthal mosaicity [39,41,42]. After longer deposition times (30 min instead of 10 min) at the same cell temperature, NaCl films reveal similar

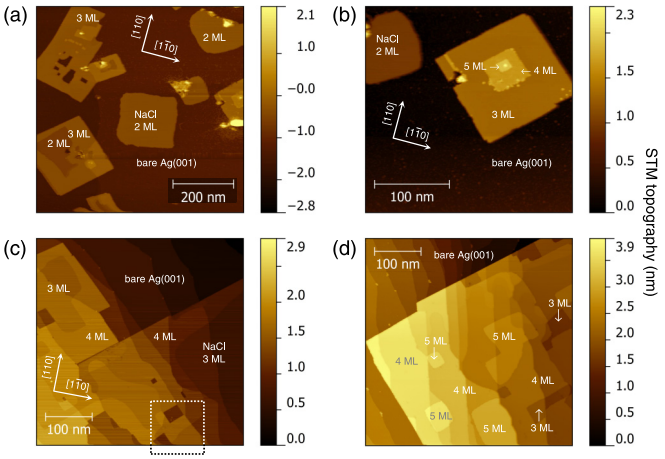

FIG. 1. STM topography of the NaCl films before electron irradiation. (a) 680×680 nm^2 image and (b) 272×272 nm^2 image ($U_b = 4$ V, $I_t = 0.7$ nA) of an ultrathin NaCl film grown on Ag(001) at 413 K (10 min deposition). (c) 435×435 nm^2 image ($U_b = 1$ V, $I_t = 0.8$ nA) and (d) 435×435 nm^2 image ($U_b = 4$ V, $I_t = 0.12$ nA) of two ultrathin NaCl films grown at 500 K, differing in nominal thickness by a factor of 4 to 5 (according to AES measurements), the latter is the thickest. All STM images are recorded at low temperature (78 K). The NaCl film thickness in atomic monolayers (ML), as determined from the STM height variations, and the orientation of the [1$\bar{1}$0] and [110] axes of Ag(001) is indicated in the images.

features with larger side lengths, in the 200–500 nm range (data not shown here).

Figures 1(c) and 1(d) show STM topography images of two ultrathin NaCl films grown on Ag(001) at 500 K, which differ in nominal thickness by a factor of 4 to 5 (according to AES measurements), respectively. On both samples, the STM images reveal large NaCl domains, exceeding 1 μm^2 in area and surrounded by large bare Ag(001) areas. The outer edges of these domains are straight and oriented at $\approx$45° to the [1$\bar{1}$0] and [110] axes of Ag(001). As previously reported, this is consistent with NaCl(001) domains having their crystallographic directions parallel to those of Ag(001) on average (comparatively low azimuthal mosaicity is expected at this growth temperature [42]) and nonpolar edges [41] composed of alternating Cl^- and Na^+ ions.

The local thickness of the NaCl domains, i.e., the number of atomic monolayers (ML), is determined from the apparent height measured by STM at different bias voltages [43,44] (see STM height profiles in Ref. [40]) and comparison with previous STM [38] and noncontact atomic force microscopy [39] studies. Cabailh *et al.* [39] observed that NaCl films grown on Ag(001) at substrate temperatures in the 343–443 K range essentially consist of $\geqslant$ 2 ML-thick islands. At low bias voltage ($U_b = 1$ V), in the area shown in Fig. 1(b), we measure STM heights of 0.30, 0.42, 0.53 and 0.65 nm, that we assign to thicknesses of 2, 3, 4 and 5 ML. This is consistent with STM heights of 0.310 and 0.460 nm for 2- and 3-ML NaCl/Ag(001) reported by Ploigt *et al.* [38].

STM spectroscopy and atomic-resolution STM images reveal that, at low bias ($U_b = 1$ V), electrons tunnel from the tip to metal-induced gap states at the NaCl/Ag(001) interface [43,45,46] (see Ref. [40]). The apparent thickness of the NaCl

atomic layers beyond 2 ML in STM images (0.12 ± 0.02 nm) is lower than the expected value (0.282 nm). At higher voltage bias $U_b = 4$ V, the 2 ML NaCl/Ag(001) shows a measured height of 0.90 nm and the apparent thickness of the next NaCl layers up to 6 ML is 0.30 ± 0.02 nm, which is close to their true thickness. In these conditions, electrons tunnel to an image potential state above the Ag(001) surface, which is possible at $U_b = 4$ V because the first field emission resonance is shifted in energy from about 4.5 to 3.3 eV upon NaCl adsorption [38] (see STM spectroscopy data in Ref. [40]). In addition, we observe in Figs. 1(c) and 1(d) that NaCl growth at 500 K yields thicker islands, compared to those grown at 413 K, with most islands consisting of large 3- to 5 ML-thick NaCl domains.

Dark areas within islands, in Figs. 1(a) and 1(c), are identified as holes. In NaCl films grown at 413 K, the irregular polygonal shapes of these holes indicate the coalescence of smaller NaCl islands that have different azimuthal orientations, that form during the film growth. Holes with more regular, almost perfectly rectangular shapes are seen in STM images of NaCl films grown at 500 K (see area inside the dotted line in Fig. 1(c) and Ref. [40]). We assume that this is due to lower azimuthal mosaicity and that hole formation is also driven by coalescence of azimuthally mismatched islands.

B. Cl depletion kinetics

The chemical modification of the ultrathin NaCl film upon electron irradiation is investigated using AES. We monitor the evolution of the Cl/Ag peak ratio defined in Sec. II as a function of the time that the sample is exposed to the 3-keV electron beam of the AES and we compare the results obtained for various film thicknesses. Figure 2(a) shows one set of these data. We see in this graph that electron irradiation induces Cl depletion. Moreover, the data fit very well a monoexponential decay function of time $\mathrm{Cl/Ag}(t) = \alpha + \beta \exp(-\gamma t)$, where α is a constant, β is the decay amplitude, and γ is the decay rate coefficient. Analyzing all the data sets in this way provides statistics on the reaction kinetics. Figure 2(b) shows the results obtained for the NaCl films grown on Ag(001) at 500 K. The decay rate coefficient γ is plotted versus the amplitude β of the decay, which is related (if neglecting the offset by α) to the NaCl film thickness. A mean decay rate coefficient $\langle\gamma\rangle = 0.011 \pm 0.001$ s^{-1} is found (i.e., a mean lifetime $\langle\tau\rangle = \langle\gamma^{-1}\rangle = 96 \pm 15$ s^{-1}), with no significant dependence on β. Thus Cl depletion induced by electron irradiation in ultrathin NaCl films apparently follows first-order reaction kinetics during the first few hundred seconds. The offset $\alpha > 0$ in the fit, however, indicates that part of the chlorine available at the surface remains after longer irradiation times or is not depleted with the same efficiency (e.g., due to the geometry of the irradiated film). A pure first-order reaction would proceed at a rate $d[\mathrm{Cl}]/dt$ that linearly depends on Cl concentration, as follows:

$$-\frac{d[\mathrm{Cl}]}{dt} = k[\mathrm{Cl}], \tag{1}$$

$$[\mathrm{Cl}](t) = [\mathrm{Cl}](0)e^{-kt}, \tag{2}$$

where the reaction rate coefficient k can be equated with γ. This is the ideal case of a surface reaction where the reaction rate coefficient k is independent of the surface coverage. There, no offset occurs and the concentration of reactants decays monoexponentially to zero at infinite time. Nevertheless, we can estimate the efficiency of the electron interaction with NaCl, for the part that behaves like a first-order reaction, using Fig. 2(b) and Eq. (1). During AES measurements, the sample current is measured at 0.5 ± 0.2 μA and the electron beam spot has a diameter of about 1 mm^2, which corresponds to an incident electron flux φ_e of about 4×10^{12} electron mm^{-2} s^{-1}. This is compared with the surface density of Cl atoms ρ_{Cl} in the NaCl(001) plane of about 6×10^{12} mm^{-2}. Thus we obtain for a surface coverage of 1 ML, a depletion rate $k\rho_{\mathrm{Cl}}\varphi_e^{-1}$ of about one Cl atom per sixty incident electrons.

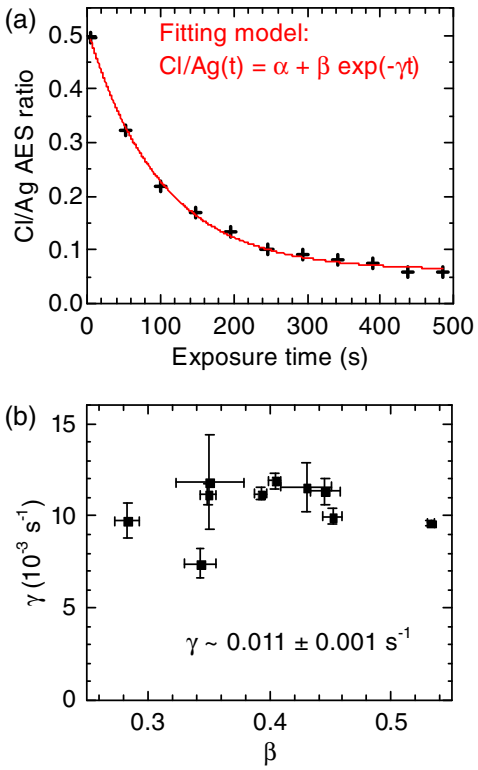

FIG. 2. NaCl dissociation dynamics upon irradiation with the 3-keV electron beam of an AES. (a) Temporal evolution of the intensity ratio between the Cl and Ag AES peaks taken at Auger electron energies of 181 and 358 eV, respectively, vs irradiation time. The sample current is 0.5 ± 0.2 μA with a beam spot area of about 1 mm^2. The experimental data are fitted using a monoexponential decay model. (b) Statistics from the model parameters yield a mean decay rate coefficient $\langle\gamma\rangle = 0.011 \pm 0.001$ s^{-1} with no significant dependence of γ on the decay amplitude β. The data shown in this figure were obtained for NaCl films grown on Ag(001) at 500 K.

C. Surface reconstruction and Na atom ordering

Controlling the outcomes of the reaction, i.e., selecting the superstructures that result from the electron-induced dissociation of alkali-halide thin films, is key in the perspective of applications. Here, we show that this aspect is strongly related to the reaction kinetics, since various superstructures occur during the course of the reaction. Remarkably, we observe all the superstructures that have been reported in previous studies

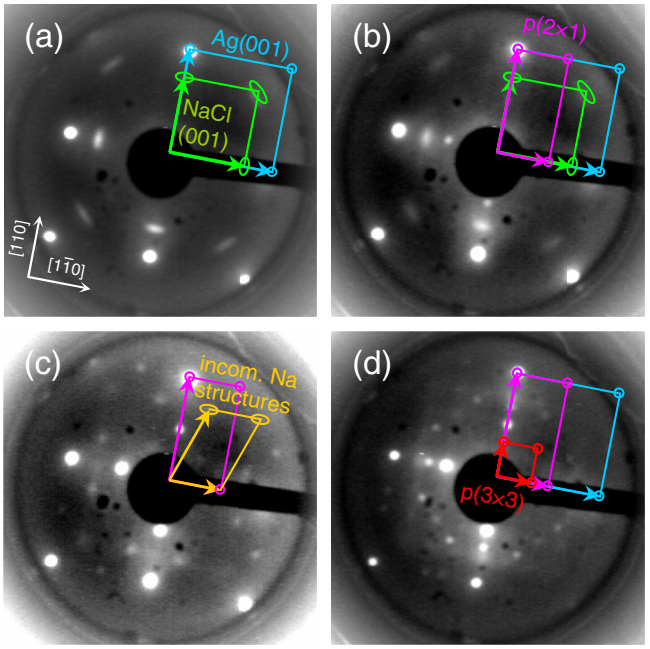

FIG. 3. Background-subtracted LEED images, obtained from ultrathin NaCl films grown on Ag(001) at 500 K. (a) NaCl on Ag(001) before dissociation. (b) Appearance of a $p(2 \times 1)$ structure in the early steps of NaCl dissociation, attributed to missing-row reconstruction of the substrate surface. (c) Longer exposure to low-energy electrons [images (b) and (c) are separated in time by 218 s] yields almost complete disappearance of the NaCl spots and appearance of an incommensurate structure (weak elongated spots), attributed to 1D chains of Na atoms adsorbed on the reconstructed substrate. (d) Starting from a thicker NaCl film yields a $p(3 \times 3)$ structure, which is associated to the formation of an ordered Ag-Na surface alloy. All LEED images measured at electron energy 52 eV, except (d) recorded at 49 eV.

of Na deposition on Ag(001), each occurring at different steps of NaCl dissociation and with some dependence on the initial NaCl film thickness. Below, we show the results obtained from the NaCl films grown on Ag(001) at 500 K, which are then compared with the results obtained from those grown at 413 K (shown in Ref. [40]).

Figure 3 shows experimental LEED images measured at different times during the reaction induced by the incident low-energy (52 eV) electrons. AES measurements carried out afterward on different (not previously irradiated) areas of the sample indicate Cl/Ag peak ratios of 0.2 and 0.5 for the NaCl films examined in Figs. 3(a) and 3(d), respectively. In the first seconds of irradiation [see Fig. 3(a)], the LEED pattern exhibits nothing but the diffraction spots of the substrate and those of the NaCl film. The latter confirms our STM observations, i.e., the presence of (001)-terminated NaCl domains with on average parallel orientation with respect to Ag(001) and low azimuthal mosaicity (elongated shape of the NaCl spots). Soon after, the first-order diffraction spots of a $p(2 \times 1)$ superstructure (and of its rotation-invariant) appear [see Fig. 3(b)]. Comparison with previous work on Na adsorption on Ag(001) [29] allows the $p(2 \times 1)$ superstructure to be assigned to a missing-row reconstruction of the Ag(001) surface.

As the sample is further irradiated, additional superstructures are observed, which differ depending on the initial film thickness. In addition, the relative intensity of the background in the LEED images increases, which indicates an increasing disorder. The electron-induced disorder in the NaCl film is further discussed in Sec. III E. In Fig. 3, the background is subtracted from the LEED images in order to improve the visibility of the diffraction spots of the ordered structures. In the LEED image shown in Fig. 3(c), which was recorded 218 s after that shown in Fig. 3(b), the NaCl spots have almost completely vanished and the pattern of an incommensurate structure is observed. The latter is characterized by weak and slightly elongated spots, as illustrated in the model. Such features have already been reported for the Na/Ag(001) system [33] and interpreted as linear incommensurate chains of Na atoms ordered in the missing rows of the reconstructed silver surface. When a slightly thicker NaCl film is irradiated, we observe that the incommensurate structure mentioned above coexists with a commensurate $p(3 \times 3)$ [see Fig. 3(d)] or $p(4 \times 2)$ structure [see Fig. 4(b)]. In a previous study of the Na/Ag(001) system, the (3×3) superstructure was identified as a 2D ordered Na-Ag surface alloy [29]. This results from a different type of missing-row reconstruction of Ag(001), where every third atomic row along the two orthogonal directions of the top substrate layer is substituted by Na atoms. The (4×2) superstructure has also been produced through Na deposition on Ag(001), but its precise nature has not yet been elucidated.

Conducting similar experiments on the NaCl films grown at 413 K yields similar results as those detailed above (see LEED images in Ref. [40]), except that the (4×2) superstructure and the incommensurate chains are not observed within the investigated irradiation time (500 s). In addition, the (3×3) superstructure is only visible for the thickest film (30 min deposition), which confirms the dependence on the film thickness and/or geometry.

D. Kinetics of structural changes

Upon electron irradiation, both the chemical and the structural properties of the ultrathin NaCl films evolve, producing different LEED patterns in a time sequence. Interestingly, these diffraction patterns can be assigned to superstructures previously reported for the Na/Ag(001) system. We show below that they appear in a specific time order, with some of the superstructures occurring simultaneously and others sequentially. This is revealed by monitoring diffraction spot intensity while irradiating the sample using the LEED.

Figure 4 shows the results obtained for two ultrathin NaCl films grown on Ag(001) at 500 K, which differ by a factor $\approx$4 in nominal thickness according to AES measurements, with a Cl/Ag($t = 0$) ratio of 0.5 for the film shown in Figs. 4(a) to 4(c) and 0.12 for that in Fig. 4(d). At time $t = 0$ (before any irradiation), the LEED patterns exhibit the expected Ag(001) and NaCl(001) spots. On the thicker NaCl film, a rapid onset of the $p(2 \times 1)$ superstructure is observed almost from the beginning of the irradiation. On both NaCl films considered in Fig. 4, the intensity of the $p(2 \times 1)$ LEED pattern varies with time and its time derivative abruptly changes value (or even sign) during the first 400 s of irradiation, before it seemingly

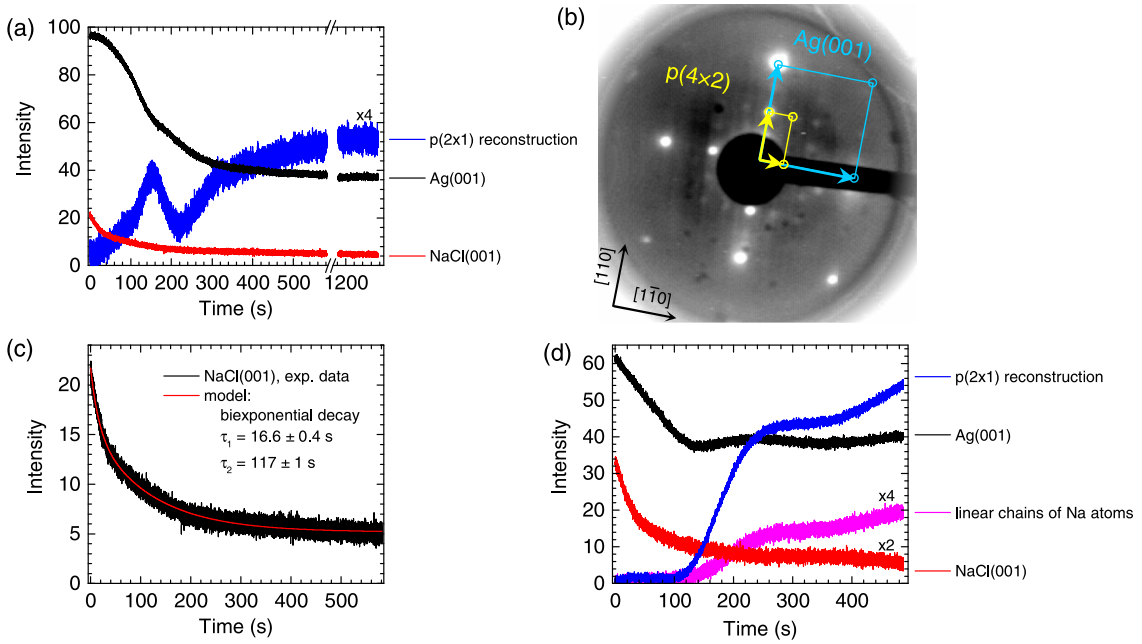

FIG. 4. LEED spot intensity vs time, measured on ultrathin NaCl films grown on Ag(001) at 500 K. [(a),(c),(d)] Temporal variations of the diffraction spots upon irradiation with the electron beam of the LEED. The intensity of the ($\bar{1}$,0) spots is monitored for the Ag(001) surface and its $p(2 \times 1)$ missing-row reconstruction and for the (001)-terminated NaCl film, whereas intensity is averaged over several spots for the linear incommensurate chains of Na atoms. In (a), the time axis features a 600 s break during which the electron beam is blocked, before irradiation restarts at $t \approx 1180$ s. (b) Background-subtracted LEED image recorded at electron energy 60 eV during the same experiment as in (a) at $t \approx 1250$ s and revealing a $p(4 \times 2)$ superstructure. In (c), the temporal variation of the NaCl spot intensity [same data as in (a)] is fitted with a biexponential decay function with optimized short (τ_1) and long (τ_2) time constants. In order to improve visibility, some of the data are multiplied by 2 or 4 [when indicated in (a) and (d)]. As a relative thickness indication, AES measurements give Cl/Ag($t = 0$) at 0.5 for the NaCl film considered in (a) to (c) and 0.12 for that used in (d). LEED measurements and irradiation were conducted at electron energy of 60 eV for the thicker film and 53 eV for the thinner one.

reaches a plateau. In Fig. 4(a), the sample is irradiated for 580 s and then the electron beam is blocked for 600 s; after this period, the sample is exposed again to electrons and we measure the LEED image shown in Fig. 4(b). The intensity values before and after the break in Fig. 4(a) are comparable; at most, the curves continue to converge to their horizontal asymptotes while the sample is unexposed, presumably due to diffusion processes. In addition, the $p(4 \times 2)$ measured at $t = 1250$ s is already visible at $t = 575$ s (not shown), yet with a slightly lower contrast. Overall, electron irradiation seems not necessary to maintain the irradiation-induced superstructures, once a stationary state is reached.

We have reproduced these experiments on several ultrathin NaCl films grown at 500 K differing in nominal thickness and we have systematically observed the following features. Firstly, the LEED spots assigned to the (2×1) surface reconstruction and the linear chains of Na atoms adsorbed in the missing rows of the reconstructed surface vary in intensity with irradiation time in the same way. As seen in Fig. 4(d), their respective curves change slope simultaneously. The intensity of the LEED spots related to the linear Na chains is much weaker than that of the (2×1) reconstruction, which hampers their observation at some of the investigated NaCl thicknesses, especially when the background level due to the disordering of the film is comparatively strong. Secondly, the $p(3 \times 3)$ structure ascribed to surface alloying shows up later than the two above-mentioned superstructures. Finally, we observe that the intensity of the NaCl(001) spots decreases upon electron irradiation following a bi-exponential decay function of time. Attempts to fit the data with a monoexponential model fail to correctly reproduce the first ≈50 s of the decay and tri- (or higher) exponential models lead to arbitrary results (i.e., totally dependent on the initial fit parametrization). The analysis of the data from Fig. 4(a) is shown in Fig. 4(c), where the short (τ_1) and long (τ_2) time constants of the exponential decay retrieved from the fit are given. On average over nine sets of data, we obtain $\langle \tau_1 \rangle = (1.6 \pm 0.9) \times 10^1$ s and $\langle \tau_2 \rangle = (1.1 \pm 0.5) \times 10^2$ s, with a mean ratio $\langle \tau_1/\tau_2 \rangle \approx 0.10$. Expressed in terms of a fast γ_1 and a slow γ_2 rate coefficients, these read $\langle \gamma_1 \rangle = 0.09 \pm 0.06$ s^{-1} and $\langle \gamma_2 \rangle = 0.011 \pm 0.005$ s^{-1}, respectively. At the electron energy and emission current used for the LEED measurements shown in Fig. 4(c), the sample current is evaluated at $0.6 \pm 0.2 \mu$A and the electron beam spot has a diameter of about 1 mm^2. This corresponds to an incident electron flux φ_e of about 5×10^{12} electron mm^{-2} s^{-1}, which is similar to that used for AES operations described in Sec. III B. The electron mean free path in NaCl, however, is dependent on the incident electron energy and may thus be very different in LEED and AES experiments.

Figure 5 shows the results of similar experiments carried out on the NaCl films grown at 413 K. In Figs. 5(a) and 5(b), the NaCl films differ by their nominal thickness, the film in Fig. 5(b) is thicker. The same time sequence of the films grown at 500 K is presented in Fig. 5(b), with a

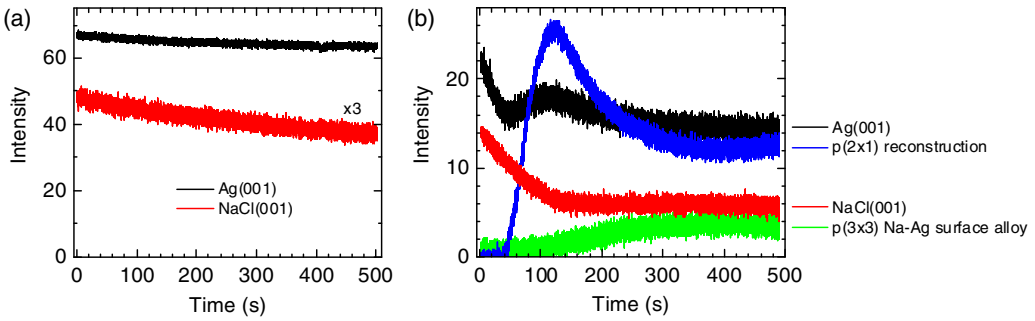

FIG. 5. LEED spot intensity vs time, measured on ultrathin NaCl films grown on Ag(001) at 413 K. Temporal variations of the diffraction spots upon irradiation with the electron beam of the LEED. The intensity of the $(\bar{1},0)$ spots is monitored for the Ag(001) surface and its $p(2 \times 1)$ missing-row reconstruction and for the (001)-terminated NaCl film, whereas intensity is averaged over several spots for the $p(3 \times 3)$ Na-Ag surface alloy. In (b), the NaCl film is thicker than in (a), since the deposition time is 30 min, as compared to 10 min at the same cell temperature in (a).

similar time evolution in the intensity variations of the LEED spots. We observe intensity variations in the LEED pattern of the $p(3 \times 3)$ structure during electron irradiation, which are temporally off-set with respect to those of the (2×1) surface reconstruction, possibly due to a competition in their respective development. The NaCl spot intensity in Fig. 5(b) exhibits a fast decay ($\gamma_1 \approx 0.02$ s^{-1}) in the first 120 s of irradiation, followed by a comparatively much slower decay (almost a plateau). In Fig. 5(a), where the NaCl film is thinner, slower kinetics are observed, compared to Fig. 5(b), with the NaCl spot intensity decaying at a rate $\gamma_1 \approx 0.002$ s^{-1}. Several measurements were conducted on different areas of the sample with the thinnest NaCl film. In the area investigated in Fig. 5(a), no other LEED spots than those of Ag and NaCl were observed upon 500 s of electron irradiation. In some other areas, we could observe the onset of the (2×1) LEED pattern, but no other Na-Ag superstructures. The absence of the (3×3) structure after 500 s irradiation of the thinnest film may be ascribed either to the slower reaction kinetics or the limited amount of reactants.

E. Irradiation effects on NaCl film geometry

Looking at the geometry of the irradiated films in real space provides further information on the important parameters in the electron-induced modifications of the films. Figures 6 and 7 show post-irradiation STM topography images of two ultrathin NaCl films grown on Ag(001) at 413 K, which differ in nominal thickness (the NaCl film is thicker in Fig. 7 than in Fig. 6). The electron beam, which is about 1 mm in diameter at the sample, is focused on selected areas along a median line of the sample (the top side of the silver crystal is 6 mm in diameter). Thus the effect of the electron dose can be investigated in STM by exploring the surface of the crystal at various distances from this median line. In Figs. 6 and 7, the irradiation time is 600 s. The modified geometry of the thinnest NaCl film, at the center of the irradiated area, where the electron dose is the highest, is shown in Figs. 6(a) and 6(b).

Despite the apparent disorder, one can distinguish the shape or the contour of the NaCl islands (see I in Fig. 6), as well as the step edges of the substrate (II). The NaCl islands exhibit nanometric holes (III), whose branchlike shape strongly differs from that of the holes seen in STM images of the as-grown NaCl films. We ascribe these holes to material removed by the electron-induced dissociation of NaCl. Between the NaCl islands, the silver surface is decorated with tiny dots which, in most cases, exhibit no long-range order. The structure of these dots is not resolved at $U_b = 4$ V, due to the delocalization of the image potential states [38]. As shown in Fig. 7(d), higher lateral resolution is obtained at $U_b = 1$ V and we observe that the dots consist of single molecules or aggregates. Most of the aggregates in Fig. 7(d) have the apparent height expected for a 1-ML NaCl layer (180 pm) [38]; however, STM spectroscopy reveals the mixed nature of some of the disordered areas.

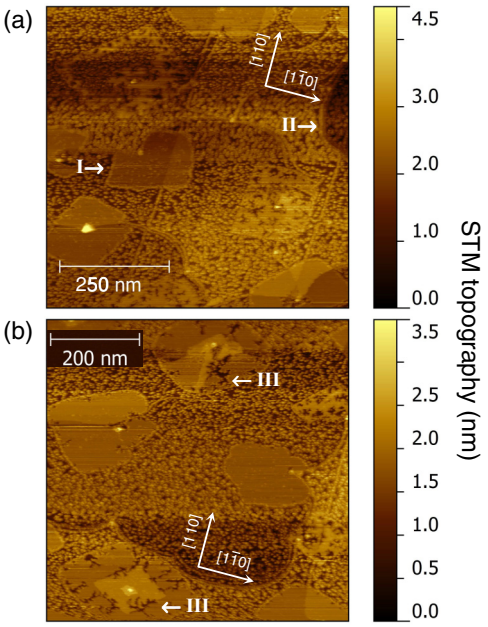

FIG. 6. STM topography of NaCl films after electron irradiation. [(a) and (b)] 680 × 680 nm^2 images ($U_b = 4$ V, $I_t = 0.7$ nA) of an ultrathin NaCl film grown on Ag(001) at 413 K (10 min deposition) after 600 s electron irradiation using the electron beam of the LEED (electron energy 52 eV) at sample current of 0.40 mA. All STM images are recorded at low temperature (78 K). The orientation of the $[1\bar{1}0]$ and [110] axes of Ag(001) is indicated in the images. (I) NaCl island contour; (II) substrate step edge; and (III) branch-shaped holes.

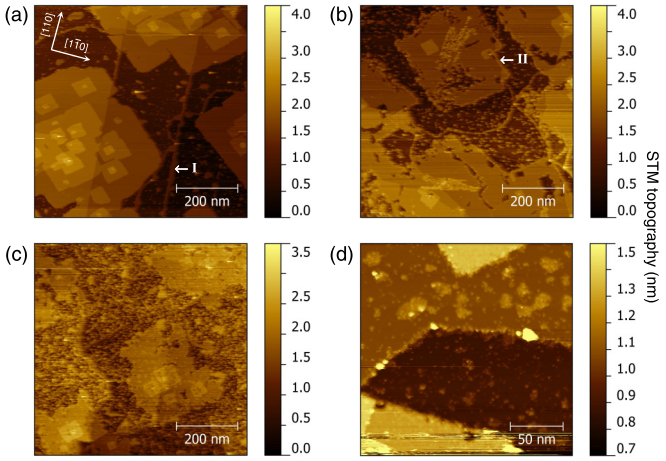

FIG. 7. STM topography of NaCl films after irradiation at different electron doses. [(a)–(c)] 680 × 680 nm^2 images ($U_b = 4$ V, $I_t = 0.7$ nA) of an ultrathin NaCl film grown on Ag(001) at 413 K (30 min deposition) after 60 s electron irradiation using the electron beam of the LEED (electron energy 52 eV) at sample current of 0.40 mA. The three images are obtained on different areas of the sample, at the center and the periphery of the irradiated zone, which have thus received different electron doses (the electron beam is about 1 mm in diameter at the sample and the top side of the sample is 6 mm in diameter). The effective electron dose increases from (a) to (c) in this figure. (d) 197 × 197 nm^2 image ($U_b = 1$ V, $I_t = 1$ nA) of the same irradiated NaCl film, revealing the geometry of the disordered areas. All STM images are recorded at low temperature (78 K). The orientation of the [1$\bar{1}$0] and [110] axes of Ag(001) is indicated in the image on the left. (I) dots at the silver step edges and (II) serrated island edges.

Figure 8 shows differential conductance (dI/dV) spectra, measured in opened-loop conditions (the initial STM parameters are indicated in inset), on ultrathin NaCl films grown at 413 K before and after electron irradiation. The dI/dV spectra of the as-grown NaCl domains exhibit a characteristic energy shift of ≈1.3 eV of the first field emission resonance of Ag(001) induced by NaCl adsorption [38]. On the irradiated samples, not all the STM spectra measured have similar spectroscopic signatures to the as-grown NaCl islands [see the spectra measured on the dots in Fig. 8(c)]. Larger energy shifts, up to ≈1.6 eV, are also observed, which is not expected for NaCl on Ag(001). Such large shifts are consistent with previous observations for Na adsorbed on Si(001) and Ge(001) surfaces [47,48], where coverage-dependent energy shifts of the work function by up to ≈2.5 eV were reported.

The dots preferentially adsorb at the step edges of the silver substrate. Interestingly, the edges of the NaCl islands have a serrated aspect in the STM images, with a higher apparent height measured at $U_b = 4$ V compared to the island center. These observations reveal that electron irradiation induces disorder into the NaCl films, in addition to Cl depletion. We infer from Fig. 6 that this disorder is due to the removal of NaCl molecules from the island edges, which diffuse and adsorb on the substrate terraces and step edges. In addition, the adsorption of sodium atoms on the surface may hamper the growth of well ordered NaCl domains.

In the image sequence shown in Figs. 7(a)–7(c), the effective electron dose increases from (a) to (c). In Fig. 7(a), where the dose is the lowest, dots are visible between the islands and preferentially at the silver step edges (see I in Fig. 7); whereas, no holes are observed yet in the islands. In Fig. 7(b), where the dose is higher, the density of dots is higher and the islands have serrated edges (II). Holes are now visible in the islands. This supports the hypothesis of two distinct processes: disordering and Cl depletion.

Even though the post-irradiation STM measurements were made in the same areas as those studied using LEED, we unfortunately could not obtain within this study atomic resolution STM images showing in real space the ordered Na-Ag phases that we observe in LEED. Scanning the irradiated NaCl films at low bias without damaging the tip was extremely difficult, due to the presence of aggregates, and scanning at high voltage prevented atomic resolution, due to lateral delocalization of the image potential states. This hampered a statistical study on large areas of the sample. Nevertheless, our observations indicate that disordered areas may largely dominate over the areas of ordered Na-Ag structures; which is consistent with the comparatively strong background observed in the LEED patterns of the irradiated samples.

IV. DISCUSSION

In the bulk crystal and thick film cases, the irradiated material may be considered a virtually infinite reservoir of molecules to dissociate; in the ultrathin film case, however, the limited amount of reactants may have a strong effect on the reaction kinetics. Below, we discuss the results shown in Sec. III with the aim of elucidating what is specific to ultrathin films in the kinetics of alkali halide dissociation induced by electron irradiation.

It is generally admitted that electron irradiation of alkali halides produces defects through the creation of electron-hole pairs, whose diffusion to the surface results in the desorption of particles; however, various mechanisms have been proposed, depending on the systems and the irradiation conditions (electron energy, sample temperature, surface geometry, etc.) [14,37,49]. A review of the possible electronic processes leading to defect production, stimulated desorption and surface modification in irradiated alkali halides can be found in Ref. [37]. The elementary interactions of the system include the primary excitations, which produce free excitons and hot holes, the diffusion of hot electron-hole pairs, color centers and interstitial anions, and finally the emission of halogen and alkali atoms from the surface. For instance, nonthermal desorption of halogen atoms can occur before the hot charge carriers are trapped and localized in the cristal lattice [50]. In contrast, the rearrangement of the lattice around the excitation products yields Frenkel defects, which diffuse and recombine at the surface; a process through which thermal desorption of both halogen and alkali atoms can occur [51].

The low-energy electron irradiation of cleaved KBr(001) and NaCl(001) crystal surfaces has motivated a number of studies in the past and a model has been proposed for the resulting desorption of halogen atoms. Within this model, incident electrons induce defects in the bulk (halogen vacancies and interstitial halogen atoms), which may diffuse to the

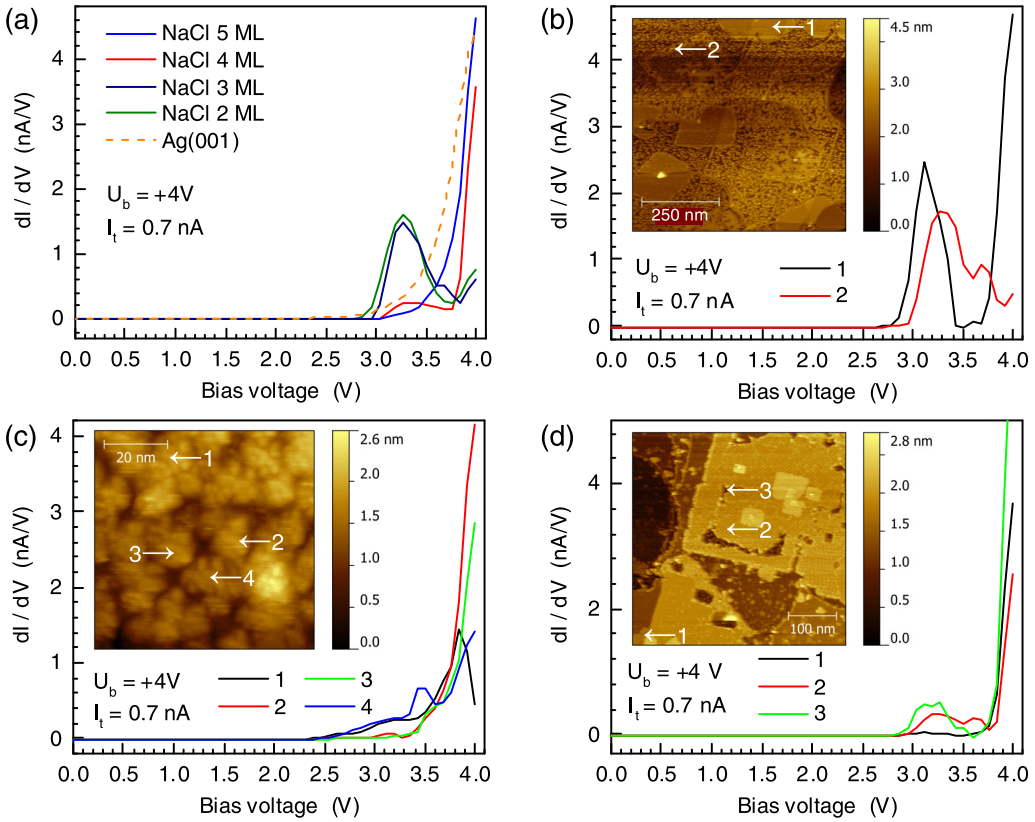

FIG. 8. Differential conductance (dI/dV) spectra of ultrathin NaCl films grown on Ag(001) at 413 K (a) before and [(b)–(d)] after electron irradiation. (a) dI/dV spectra obtained on the as-grown NaCl domains shown in Fig. 1(b), whose thickness ranges from two to five NaCl atomic layers (monolayer, ML), and on the bare Ag(001) surface. [(b) and (c)] dI/dV spectra measured on the irradiated NaCl film shown in Fig. 6(a). (d) dI/dV spectra measured on the same NaCl film as shown in Fig. 7(b). All the dI/dV spectra are measured in opened-loop conditions (the initial STM parameters are $U_b = 4$ V and $I_t = 0.7$ nA) by varying the bias voltage from 0 to 4 V by steps of 100 mV. The dI/dV spectra are measured at the position indicated by the apex of the arrows in the STM images ($U_b = 4$ V, $I_t = 0.7$ nA) shown in inset. All STM images are recorded at low temperature (78 K).

surface where halogen atoms are ejected out of the plane and alkali metal atoms aggregate into metallic clusters [15,52–55]. Although this model suggests that electron induced desorption of alkali halide surfaces essentially leads to halogen atom removal, similar kinetics and desorption fluxes have been reported for halogen and alkali metal atoms [14,15,37,55]. This has been explained by surface diffusion of alkali metal atoms to step edges of the alkali-halide surface, where electron-stimulated desorption of alkali metal atoms is more efficient [53–55]. As a result, the desorption kinetics are correlated with the surface density of step edges. In particular, alkali-halide desorption from cleaved crystal surfaces has been shown to proceed layer by layer, which results in a periodic variation of the step density with period corresponding the removal of one atomic layer, and the same periodic oscillations were observed in both the desorption fluxes of halogens and alkali metals [37,53–55]. In contrast, we do not observe such oscillations in the AES data measured from ultrathin NaCl films on Ag(001), where the Cl signal mono-exponentially decays with increasing irradiation time. In addition, a significant amount of Na atoms must remain on the surface after NaCl dissociation that does not produce clusters, since our LEED measurements suggest the formation of ordered 1D chains of Na atoms and a well-ordered Ag-Na surface alloy.

The periodic variation of the step density previously observed on cleaved alkali-halide crystal surfaces irradiated with electrons is well understood. It is known from real-space AFM measurements that randomly spread rectangular holes of monolayer depth are formed, whose edges are oriented along the main crystallographic directions of the (001) plane [53,54,56,57]. It is the growth and coalescence of these holes that yield the oscillations in the step density [55].

On bulk crystals and thick films of alkali halides, the opening of holes in the top layer reveals a surface that is of the same composition and structure. In contrast, if the film is thin enough for hole opening to reveal the bare surface of the underlying metal substrate (or even more if the film is not continuous), then alkali metal atoms may diffuse to the metallic surface. If energetically favored, the adsorption of these atoms onto (or their alloying with) the metallic surface is expected to dramatically change the kinetics of the electron stimulated desorption. This interpretation of the substrate effect is consistent with a previous study of electron-irradiated NaCl films grown on GaAs(001), where the authors reported the apparent vanishing of the Na desorption process at NaCl film thickness lower than about 10 ML [35].

The oscillations observed in the desorption rates of halide and alkali metal atoms from electron-irradiated bulk alkali

halides have been modeled using damped oscillator functions [57]. Different kinetics have been reported for thick NaCl(111) films grown on mica [15]; in Ref. [15], Friedenberg and Shapira found that the surface Cl concentration as measured by AES varies as a logarithmic function of the electron irradiation time. This behavior was interpreted as a standard Elovitch-type mechanism, where the activation energy for dissociation is concentration dependent. The argument for this interpretation is that the increasing surface concentration of alkali metal atoms creates disorder, which slows down the dissociation of further alkali-halide molecules. In contrast, the AES measurements shown in Fig. 2 clearly show that Cl concentration decays exponentially upon increasing irradiation time and the data could not be fitted with either a logarithmic nor a damped oscillator function of time. Presumably, the reaction rate constant is independent of the reactant and product concentration in the ultrathin film case because alkali metal atoms diffuse to bare substrate areas where they adsorb or react, thus do not alter the environment of undissociated alkali-halide molecules as much as in the thick film case. The Cl concentration decay, however, does not drop to zero at long exposure times in Fig. 2; an offset, or slow decaying component, is observed. From the STM images of the irradiated films shown in Fig. 7, we infer that the bare substrate areas are increasingly occupied by disordered NaCl molecules removed from the NaCl islands as irradiation is pursued. A change in the reaction kinetics is thus observed when the concentration of disordered NaCl molecules starts to hamper alkali metal atom diffusion to the bare substrate areas.

To summarize briefly, the electron-induced modification of the ultrathin NaCl films proceeds in two stages. At the first reaction steps, Na diffusion on the bare substrate is not significantly affected by disorder and, thus, Cl depletion is not limited by Na accumulation on NaCl islands. After some irradiation time, however, Na diffusion is increasingly limited by disorder and this strongly slows down the reaction kinetics. Depending on the initial film thickness, this effect occurs in a more or less early phase of the reaction and this is one of the factors that determine what Na-Ag superstructures finally form.

The comparison of the kinetics revealed by AES and LEED investigations is interesting. On the one hand, a monoexponential decay is observed in the evolution of the Cl/Ag AES ratio shown in Fig. 2(a) with, however, an offset or slow decaying component, which indicates that part of the available chlorine is not desorbed with the same efficiency upon irradiation. On the other hand, the NaCl(001) LEED pattern shown in Fig. 4 decays in intensity following a bi-exponential law with fast γ_1 and slow γ_2 decay rates differing by about one order of magnitude. For the NaCl films grown at lower temperature, as shown in Fig. 5, the time trace of the NaCl spots also exhibit a fast and a slow component (for the thickest film) or a monoexponential decay with an apparent offset (for the thinnest film). Moreover, post-irradiation STM images shown in Fig. 7 reveal that a fast disordering process coexists with a comparatively slower mechanism of hole formation, which is driven by Cl depletion from NaCl islands. Within this picture, our AES and LEED observations can be understood as follows. The fast intensity decay of the NaCl LEED pattern is due to the disordering process, where electron irradiation induces NaCl removal from the NaCl island edges; whereas the slow decay component is ascribed to the increasing density of Cl vacancies (and formation of holes) in the NaCl islands. The monoexponential decay of the Cl/Ag AES ratio results from the Cl depletion from the NaCl islands and Na atom diffusion to bare silver areas, until the disordering process significantly reduces the available areas on bare Ag(001), which leads to a strong slowdown of the Cl depletion and yields a plateau in the AES data at long irradiation times.

Finally, the time sequence of the superstructures observed in LEED during the course of the dissociation reaction reveals crucial information on the mechanism through which these superstructures occur. Firstly, a missing-row $p(2 \times 1)$ surface reconstruction systematically shows up after some irradiation time, for all investigated initial nominal thickness of the NaCl film grown on Ag(001) (except the thinnest films grown at 413 K, where we do not always observe the formation of superstructures upon 500 s irradiation). The same surface reconstruction is known to occur upon adsorption of various alkali metals (Li, Na, K, Rb) on the (001) face of Cu, Ag and Au crystals [33] at room temperature (RT) in a coverage range $\Theta \approx 0.2$–0.4. Here, Θ is defined as the ratio between the number of adsorbed alkali-metal atoms over the number of atoms in a (001) plane of the substrate; thus, the first alkali-metal monolayer may be completed at $\Theta < 1$. In all of these systems, the $p(2 \times 1)$ is the first superstructure to appear at RT upon increasing Θ. Alkali-metal atoms are known to form linear incommensurate chains in the missing rows of the reconstructed metal surface in the Na/Ag(001) and Li/Cu(001) systems [23,33] at RT within a narrow coverage range, i.e., $\Theta = 0.37$–0.39 for Na/Ag(001) [33]. As well, $(n \times n)$ surface alloys (with $n = 3,4,5$) have been observed by LEED and STM measurements on several systems [33], including Li/Cu(001), Li/Ni(001) and Na/Ag(001), at RT and for $\Theta > 0.4$. Finally, the $p(4 \times 2)$ seems specific to the Na/Ag(001) system and has been obtained at RT for $\Theta > 0.55$ (Na monolayer is completed at $\Theta \approx 0.7$) [29].

Remarkably, we demonstrate that all the superstructures mentioned above may be obtained through electron-induced dissociation of ultrathin NaCl films grown on Ag(001). With the exception of the incommensurate chains, these superstructures occur within alkali-metal surface coverage ranges that do not overlap. Therefore the fact that we see two or more [e.g., the (2×1) and (4×2) in Fig. 4(b) or the (3×3) and (2×1) at $t \approx 400$ s in Fig. 5(b)] of these superstructures coexisting indicates that Na surface concentration must be highly heterogeneous. Furthermore, we see intensity oscillations in their LEED patterns (at constant sample current) as the reaction proceeds, which means that the Na surface concentration locally oscillates. The oscillations in the LEED patterns are only observed during the first 400 s on average and then the system seems to converge to an equilibrium state [as seen in Fig. 4(a)].

From the observations reported above, we conclude that, in electron-irradiated ultrathin NaCl films on Ag(001), areas where Na surface concentration can reach comparatively high values coexist with areas that are essentially covered with disordered NaCl molecules, together with the remaining parts of the initial NaCl islands. This implies that Na atom diffusion occurs within limited areas, which can be ascribed to the

accumulation of NaCl molecules at the step edges of the substrate. The slowdown in the reaction kinetics observed in LEED and AES after a few hundred seconds indicates that NaCl dissociation and Cl desorption from disordered NaCl molecules and aggregates is significantly lower than from well ordered NaCl islands. As a result, the reaction kinetics are dependent on the surface coverage rate of the ultrathin NaCl films, which will have an effect on the ratio between ordered and disordered NaCl areas. Moreover, the thickness of the NaCl islands has an effect on the electron-matter interaction efficiency, because the electron penetration depth is longer than the film thicknesses considered in this work (see discussion on the desorption yields in Ref. [40]).

V. CONCLUSIONS

In conclusion, the electron induced dissociation of ultrathin alkali-halide films grown on fcc metals differs, in terms of reaction kinetics and outcomes, from that of their thick film and bulk crystal counterparts. These differences mainly ensue from the limited amount of reactants and the product interactions with the substrate. At sufficiently low thickness (typically 2 to 5 ML), alkali-halide films on metals may be discontinuous and/or exhibit holes, especially when their growth involves the coalescence of domains with mismatched orientations. Additional holes are expected to be formed upon electron irradiation, due to the creation of supplementary defects in the film. Therefore, the alkali metal atoms produced from alkali-halide dissociation do not only aggregate in metallic clusters at the step edges, but also diffuse to bare areas of the metallic substrate, where they adsorb and can form superstructures or undergo alloying reactions.

All the superstructures that are known to be produced through deposition of Na atoms on Ag(001) were observed in LEED during the dissociation of ultrathin NaCl films grown on Ag(001). These superstructures, which include reconstructions of the Ag(001) surface and a 2D Na-Ag alloy, have their relative coverage varying in time during the first minutes of irradiation, due to local variations in the Na concentration. This indicates that the observed Na-Ag superstructures are *metastable*. This implies that the phase transitions between two of these Na-Ag superstructures is reversible, even though they exist over different ranges of Na concentration. This could not be demonstrated in the previous studies based on Na deposition on Ag(001), because the surface concentration in Na was monotonously increased.

In addition, the electron irradiation induces an increasing disorder in the ultrathin NaCl films, which slows down the reaction kinetics of both the dissociation of NaCl and the formation of Na superstructures on silver; as a result, the reaction kinetics and products depend on the NaCl film thickness. In the conditions used in this study, the disordered areas are found to strongly dominate the geometry of the electron irradiated films. Further investigations are necessary to control the ratio between the disordered and ordered areas, before electron irradiated alkali-halide ultrathin films can eventually be used as "templates" for anchoring single organic molecules or producing macromolecular structures on a surface [58–62].

ACKNOWLEDGMENTS

This work is supported by a public grant from the LabEx PALM overseen by the French National Research Agency (ANR) as part of the "Investissements d'Avenir" program (ANR-10-LABX-0039). This work is part of the M-Exc-ICO project, which is supported by a public grant from the ANR (ANR-16-CE24-0003). A.H. acknowledges financial support from the Campus France agency through a PhD fellowship.

[1] R. Bennewitz, J. Phys.: Condens. Matter **18**, R417 (2006).
[2] P. Myrach, N. Nilius, and H.-J. Freund, Phys. Rev. B **83**, 035416 (2011).
[3] G. Sitja, S. Le Moal, M. Marsault, G. Hamm, F. Leroy, and C. R. Henry, Nano Lett. **13**, 1977 (2013).
[4] A. Yu, S. Li, G. Czap, and W. Ho, Nano Lett. **16**, 5433 (2016).
[5] J. Repp, G. Meyer, S. M. Stojković, A. Gourdon, and C. Joachim, Phys. Rev. Lett. **94**, 026803 (2005).
[6] F. Rossel, M. Pivetta, and W.-D. Schneider, Surf. Sci. Rep. **65**, 129 (2010).
[7] T. Leoni, O. Guillermet, H. Walch, V. Langlais, A. Scheuermann, J. Bonvoisin, and S. Gauthier, Phys. Rev. Lett. **106**, 216103 (2011).
[8] M. Müller, E. Le Moal, R. Scholz, and M. Sokolowski, Phys. Rev. B **83**, 241203 (2011).
[9] H. Imada, K. Miwa, M. Imai-Imada, S. Kawahara, K. Kimura, and Y. Kim, Nature (London) **538**, 364 (2016).
[10] Y. Zhang, Y. Luo, Y. Zhang, Y.-J. Yu, Y.-M. Kuang, L. Zhang, Q.-S. Meng, Y. Luo, J.-L. Yang, Z.-C. Dong, and J. G. Hou, Nature (London) **531**, 623 (2016).
[11] W. Steurer, J. Repp, L. Gross, I. Scivetti, M. Persson, and G. Meyer, Phys. Rev. Lett. **114**, 036801 (2015).
[12] S. Günther, R. Reichelt, J. Wintterlin, A. Barinov, T. O. Menteş, M. A. Niño, and A. Locatelli, Appl. Phys. Lett. **93**, 233117 (2008).
[13] S. Günther, S. Böcklein, R. Reichelt, J. Wintterlin, A. Barinov, T. O. Menteş, M. A. Niño, and A. Locatelli, Chem. Phys. Chem. **11**, 1525 (2010).
[14] H. Tokutaka, M. Prutton, I. G. Higginbotham, and T. E. Gallon, Surf. Sci. **21**, 233 (1970).
[15] A. Friedenberg and Y. Shapira, Surf. Sci. **87**, 581 (1979).
[16] E. Paparazzo and N. Zema, Surf. Sci. **372**, L301 (1997).
[17] K. Aït-Mansour, M. Bielmann, O. Gröning, P. Ruffieux, R. Fasel, and P. Gröning, Appl. Surf. Sci. **252**, 6368 (2006).
[18] R. Marbrow and R. Lambert, Surf. Sci. **61**, 317 (1976).
[19] R. Marbrow and R. Lambert, Surf. Sci. **61**, 329 (1976).
[20] A. Schmalz, S. Aminpirooz, L. Becker, J. Haase, J. Neugebauer, M. Scheffler, D. R. Batchelor, D. L. Adams, and E. Bøgh, Phys. Rev. Lett. **67**, 2163 (1991).
[21] C. Stampfl, M. Scheffler, H. Over, J. Burchhardt, M. Nielsen, D. L. Adams, and W. Moritz, Phys. Rev. Lett. **69**, 1532 (1992).

[22] J. Barth, H. Brune, R. Schuster, G. Ertl, and R. Behm, Surf. Sci. **292**, L769 (1993).
[23] S. Mizuno, H. Tochihara, and T. Kawamura, Surf. Sci. Lett. **292**, L811 (1993).
[24] R. Fasel, P. Aebi, J. Osterwalder, L. Schlapbach, R. G. Agostino, and G. Chiarello, Phys. Rev. B **50**, 14516 (1994).
[25] S. Mizuno, H. Tochihara, A. Barbieri, and M. A. Van Hove, Phys. Rev. B **52**, R11658 (1995).
[26] J. Barth, R. Behm, and G. Ertl, Surf. Sci. **341**, 62 (1995).
[27] W. Berndt, D. Weick, C. Stampfl, A. Bradshaw, and M. Scheffler, Surf. Sci. **330**, 182 (1995).
[28] H. Meyerheim, S. Pflanz, R. Schuster, and I. Robinson, Phys. B: Cond. Mat. **221**, 134 (1996).
[29] M. Imaki, S. Mizuno, and H. Tochihara, Surf. Sci. **357**, 145 (1996).
[30] H. Jiang, S. Mizuno, and H. Tochihara, Surf. Sci. **380**, L506 (1997).
[31] H. Meyerheim, I. Robinson, and R. Schuster, Surf. Sci. **370**, 268 (1997).
[32] S. Mizuno, H. Tochihara, Y. Matsumoto, and K. ichi Tanaka, Surf. Sci. **393**, L69 (1997).
[33] H. Tochihara and S. Mizuno, Prog. Surf. Sci. **58**, 1 (1998).
[34] A. Mikkelsen and D. L. Adams, Phys. Rev. B **60**, 2040 (1999).
[35] M. Szymonski, J. Kolodziej, P. Czuba, P. Piatkowski, P. Korecki, Z. Postawa, and N. Itoh, Appl. Surf. Sci. **100**, 102 (1996).
[36] J. Kolodziej, P. Piatkowski, and M. Szymonski, Surf. Sci. **390**, 152 (1997).
[37] M. Szymonski, J. Kolodziej, B. Such, P. Piatkowski, P. Struski, P. Czuba, and F. Krok, Prog. Surf. Sci. **67**, 123 (2001).
[38] H.-C. Ploigt, C. Brun, M. Pivetta, F. Patthey, and W.-D. Schneider, Phys. Rev. B **76**, 195404 (2007).
[39] G. Cabailh, C. R. Henry, and C. Barth, New J. Phys. **14**, 103037 (2012).
[40] See Supplemental Material at http://link.aps.org/supplemental/10.1103/PhysRevB.96.235418 for STM height profiles of the as-grown NaCl films, atomic-resolution STM images of NaCl domains, LEED images of the NaCl films grown at 413 K recorded during electron irradiation, further STM images of irradiated NaCl films, additional discussion on the desorption yields evaluated from AES, and description of the experimental setup, sample preparation and data analysis methods, in more detail, which includes Refs. [63–67].
[41] M. Pivetta, F. Patthey, M. Stengel, A. Baldereschi, and W.-D. Schneider, Phys. Rev. B **72**, 115404 (2005).
[42] E. Le Moal, M. Müller, O. Bauer, and M. Sokolowski, Surf. Sci. **603**, 2434 (2009).
[43] W. Hebenstreit, J. Redinger, Z. Horozova, M. Schmid, R. Podloucky, and P. Varga, Surf. Sci. **424**, L321 (1999).
[44] Q. Guo, Z. Qin, C. Liu, K. Zang, Y. Yu, and G. Cao, Surf. Sci. **604**, 1820 (2010).
[45] R. Arita, Y. Tanida, K. Kuroki, and H. Aoki, Phys. Rev. B **69**, 115424 (2004).
[46] M. Kiguchi, G. Yoshikawa, S. Ikeda, and K. Saiki, Phys. Rev. B **71**, 153401 (2005).
[47] B. Naydenov and L. Surnev, Surf. Sci. **370**, 155 (1997).
[48] M. Tikhov, G. Boishin, and L. Surnev, Surf. Sci. **241**, 103 (1991).
[49] C. Tegenkamp, H. Pfnür, W. Ernst, U. Malaske, J. Wollschläger, D. Peterka, K. M. Schröder, V. Zielasek, and M. Henzler, J. Phys.: Condens. Matter **11**, 9943 (1999).
[50] M. Szymonski, J. Kolodziej, Z. Postawa, P. Czuba, and P. Piatkowski, Prog. Surf. Sci. **48**, 83 (1995).
[51] M. Szymonski, Rad. Eff. **52**, 9 (1980).
[52] T. Pian, M. Traum, J. Kraus, N. Tolk, N. Stoffel, and G. Margaritondo, Surf. Sci. **128**, 13 (1983).
[53] B. Such, P. Czuba, P. Piatkowski, and M. Szymonski, Surf. Sci. **451**, 203 (2000).
[54] B. Such, J. Kolodziej, P. Czuba, P. Piatkowski, P. Struski, F. Krok, and M. Szymonski, Phys. Rev. Lett. **85**, 2621 (2000).
[55] J. Kolodziej, B. Such, P. Czuba, F. Krok, P. Piatkowski, P. Struski, M. Szymonski, R. Bennewitz, S. Schär, and E. Meyer, Surf. Sci. **482-485, Part 2**, 903 (2001).
[56] R. Bennewitz, S. Schär, V. Barwich, O. Pfeiffer, E. Meyer, F. Krok, B. Such, J. Kolodzej, and M. Szymonski, Surf. Sci. **474**, L197 (2001).
[57] M. Goryl, B. Such, F. Krok, K. Meisel, J. Kolodziej, and M. Szymonski, Surf. Sci. **593**, 147 (2005).
[58] W. Ernst, M. Eichmann, H. Pfnür, K.-L. Jonas, V. von Oeynhausen, and K. H. Meiwes-Broer, Appl. Phys. Lett. **80**, 2595 (2002).
[59] T. K. Shimizu, J. Jung, H. Imada, and Y. Kim, Angew. Chem., Int. Ed. Engl. **53**, 13729 (2014).
[60] Q. Guo, M. Huang, S. Lu, and G. Cao, Nanotechnology **26**, 275603 (2015).
[61] J. Hieulle, D. Peyrot, Z. Jiang, and F. Silly, Chem. Commun. **51**, 13162 (2015).
[62] C. Zwick, A. Baby, M. Gruenewald, E. Verwüster, O. T. Hofmann, R. Forker, G. Fratesi, G. P. Brivio, E. Zojer, and T. Fritz, ACS Nano **10**, 2365 (2016).
[63] X. Sun, M. P. Felicissimo, P. Rudolf, and F. Silly, Nanotechnology **19**, 495307 (2008).
[64] X. Sun and F. Silly, Appl. Surf. Sci. **256**, 2228 (2010).
[65] T. Pian, N. Tolk, M. Traum, J. Kraus, and W. Collins, Surf. Sci. **129**, 573 (1983).
[66] C. D. Wagner, L. E. Davis, and W. M. Riggs, Surf. Interface Anal. **2**, 53 (1980).
[67] D. Nečas and P. Klapetek, Cent. Eur. J. Phys. **10**, 181 (2012).